

Numerical Simulation of Peristaltic Urine Flow in a Stented Ureter

Tyler Bevan¹, Rupp Carriveau^{1*}, Lee Goneau^{2,3}, Peter Cadieux²⁻⁴, and Hassan Razvi^{2,4}

¹Department of Civil and Environmental Engineering, University of Windsor, Windsor, Ontario, Canada

²Lawson Health Research Institute, London, Ontario, Canada

³Departments of Microbiology and Immunology, University of Western Ontario, London, Ontario, Canada

⁴Surgery, University of Western Ontario, London, Ontario, Canada

***Corresponding Author:**

Rupp Carriveau

Department of Civil and Environmental Engineering

University of Windsor

Windsor, Ontario

Canada

Tel: 519 253 3000

E-mail: rupp@uwindsor.ca

Received: 13 February 2012; | Revised: 10 June 2012; | Accepted: 19 June 2012

Abstract

The capacity of ureteral stents to enhance the conveyance of urine from kidney to bladder is the critical function for patients that require them. The flow path in and around the stent is not a trivial one, particularly if some elements of peristalsis are present in the ureter. This paper details a numerical flow simulation for an axially symmetric stented ureter segment. The flow of urine through a stented, elastically-modeled ureter was considered under varying pressure gradients, bore (lumen) obstructions, and peristaltic deflections (waves). Peristaltic waves are combined with the pressure gradient developed between the kidney and bladder to provide a more accurate representation of the complex flow mechanics found within the ureter. Although it is recognized that peristalsis ceases or diminishes greatly after prolonged presence of a stent, in the time frame that it is active, detrimental consequences like reflux may occur. Several relationships from varying control parameters are determined to predict the onset of reflux as flow conditions within the ureter change. It was determined that occurrence of reflux is more likely as the peristaltic deflection or the obstruction of the stent bore increases. The threat of reflux is low if the pressure gradient between the kidney and bladder remains large. These simulations provide insight into the fluid behaviour within a stented ureter that could lead to optimized stent designs and reduce the possibility of reflux, infection, and discomfort.

Keywords: Ureteral Stent Simulation, Peristaltic Flow, Reflux, Biofluid-Structure Interaction, Multiphysics Model

1. Introduction

Stents are used to create clear urinary passage from the kidney to the bladder and are a common solution to damaged or blocked ureters [1-3]. A better understanding of the complex flow involved in urine transport through a stented ureter would provide insight for improved designs to enhance patient health and comfort [3].

In a healthy body, urine collects in the kidney and passes through the ureter to the bladder where it is stored until excretion. Normal ureteral flow mechanics are a combination of peristaltic deflection of the ureteral wall and pressure differential between the kidney and bladder. Tissue damage to the ureter wall or obstruction in the vessel will greatly impede healthy flow. A blocked ureter could result in high pressures within the kidney, possibly causing infection/or and kidney failure [4-5]. When adequate flow cannot be produced or a blockage is unable to be removed, a stent is typically used to relieve the strain on both the ureter and kidney [1, 4-6].

Stents are available in a large array of materials and designs, each for a specific application. Ureteral stents are commonly a flexible, cylindrical length of synthetic polymeric composite with a central bore down its axis. The bore provides a clear path for urine to flow through in addition to the space existing between the outer stent surface and ureter wall. Stents are often coated with a smooth organic, hydrophilic material to reduce flow resistance and biofilm development. To improve the functionality of this stent design, perpendicular passages (holes) are implemented at various orientations between the annulus and bore to bypass any future obstructions that may develop. Once implanted, the stent must remain in position for the duration of its use. The most common stent design is anchored in situ by retaining coils that protrude into the kidney and bladder referred to as pig-tails [1, 3, 6].

While stents are often the best solution to enhance or even create the necessary urine passage between the kidney and bladder, complications with the indwelling device are not uncommon. Often an improperly installed or incorrectly sized stent can result in irritation of the

bladder and induce spasms and patient discomfort. Biofilm and encrustation development can also become serious concerns in longer-term implants. The adherence of bacteria, yeast and urinary precipitates may result in device infection, urinary blockages and tissue damage, often necessitating device removal or additional endoscopic or surgical procedures. However, even in the absence of these complications, stent indwelling alone poses patient risk as the natural function of the junction between the ureter and bladder is compromised. Simply put, with the stent in place, the junction can no longer close the passage between the two. This enables fluid to travel in the reverse direction from bladder to kidney; commonly referred to as reflux. Voiding of the bladder while this junction is prevented from closing can move bacteria and biofilms upstream to the kidney, risking infection (pyelonephritis) that can further lead to kidney failure and even sepsis[2, 6-10].

Research has been conducted to uncover the flow characteristics of urine through the ureter considering differential pressures and peristalsis as the motive force, both independently and combined. Modeling of flow through a stented ureter has been investigated by others using solely pressure differential as the flow mechanism [4, 11-12]. However, to our knowledge both peristaltic and differential pressure has yet not been addressed in the literature of stented ureters. In the presence of a stent, peristalsis is greatly inhibited and is sometimes considered negligible in comparison to the propulsive pressure gradient between the kidney and bladder[2, 10, 13]. Though, on an all-encompassing scale, just the slightest reflux could result in serious infection, a critical scenario potentially realized in the presence of peristalsis.

This paper extends the models of Tong, Sparrow and Abraham [11] to incorporate peristaltic deflection of the ureter wall. The intent is to investigate potential conditions that generate backflow in a very common stent design. It is assumed that the axial orientation of the stent and ureter are concentric and axially symmetric. The stent is treated as a rigid cylinder with passages to the annulus region having the same diameter as the bore, where the ureter wall is a linear

distensible representation [5]. Model physics are fully coupled to allow complete fluid structure interaction between material domains. The annulus and bore of the fluid domain at each end are defined as open sources with a pressure difference between the inlet and outlet of the ureter. Peristaltic deflection is determined by an applied Gaussian pressure distribution along the outer radius of the ureter to approximate the rise and dwell observed *in vivo* [14-15]. A blockage is also introduced into the bore and its cross-sectional area varied. Several scenarios are simulated numerically and the results discussed in detail regarding the conditions for reflux.

2. Model

Throughout this paper, several stented-ureter models have been developed to explore the conditions required for the onset of reflux in the ureter. Three geometric scenarios are introduced, over which several key variables are parameterized. All notation used to describe the models used are provided in Table 1. The first

model is of a stent in a ureter with no passages for permeation of urine between the bore and annulus fluid domains. The remaining two are modeled with a passage between the bore and annulus in which one model is fitted with a blockage within the bore of the stent. All models are created in 2D polar coordinates, (r, z) , and share the same geometric shape and dimensions with the exception of the blockage in the third model.

The length of each model, l , represents a section of length of a stented ureter where $z = 0$ at the inlet and $z = l$ at the outlet. Inlet and outlet pressures have been scaled to preserve the full ureteral length pressure gradient [11]. The ureter has an inner radius of a_i and a wall thickness of a_t coupled with a stent having an inner radius of b_i and outer radius b_o . The ureter and stent are assumed to be axially symmetrical and concentric with one another having a constant cross-sectional area along length l . Passage holes in the stent are of radius c_i where, throughout this paper, $c_i = b_i$. Blockage in the bore is of length l_b and has a radial distance from the axis of symmetry of b_b .

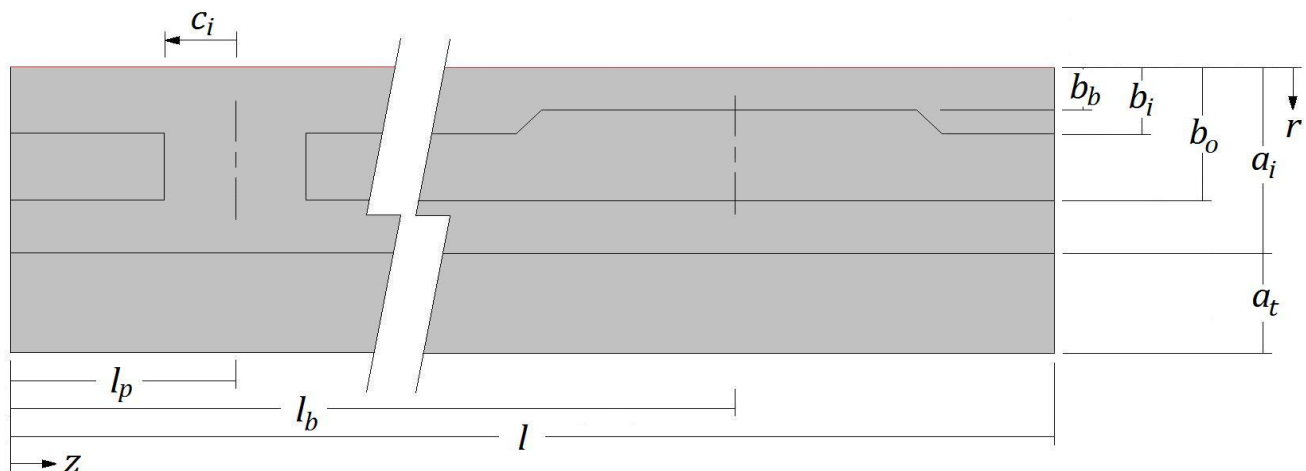


Figure 1: Model notation.

Each model is a fully coupled fluid structure interaction between the urine, stent and ureter wall. The fluid domain is treated as a homogeneous, incompressible Newtonian fluid having a density of ρ_f and dynamic viscosity of μ . Fluid flow through the domain is driven by two mechanisms; the first of which being the pressure

gradient determined by the inlet and outlet pressures, p_i and p_o , respectively. Fluid velocities developed are denoted as u and w for respective axial and radial components. The second mechanism for flow is dependent on the deflection of the ureter wall and is represented by the Gaussian function

$d(t) = p_d \cdot \exp(-(z - v \cdot t)^2 / (2 * (h/8)^2))$
 which defines the depth, position and velocity of the deflection profile. The depth of deflection is controlled through the parameter p_d , which is the pressure applied at the center of the Gaussian distribution against the outer wall of the ureter. Position of the deflection is dependent on the current time, t , and peristaltic velocity, v . The variable h controls the width of the deflection profile. The ureter wall itself is assumed to be an isotropic, homogeneous, linear elastic material model with an elastic modulus of E and Poisson's ratio of ν . The stent is assumed to be of rigid construction and fixed in relation to the ureter. All boundaries between the fluid and solid domains are assumed as no-slip velocity boundary conditions.

Table 1: List of Model Notation

Notation	Description
t	Time
r	Radial coordinate
z	Axial coordinate
a_i	Inner radius of ureter
a_t	Wall thickness of ureter
b_i	Inner radius of stent
b_o	Outer radius of stent
b_b	Bore radius at blockage
c_i	Radius of passage
l	Length of ureter and stent
l_b	Location of blockage
l_p	Location of passage
u	Axial velocity
w	Radial velocity
d	Ureter wall deflection
v	Deflection profile velocity
h	Deflection profile width
p_i	Inlet Pressure

p_o	Outlet Pressure
p_d	Deflection pressure
ρ_f	Density of urine
μ	Dynamic viscosity of urine
ν	Poisson's ratio of ureter
E	Elastic modulus of ureter

Table 2: List of Parameter Values

Parameter	Values
t	0 - 4.7 s
a_i	1.4 mm
a_t	0.75 mm
b_i	0.5 mm
b_o	1 mm
b_b	$b_i * \sqrt{3/4}, b_i * \sqrt{1/2}, b_i * \sqrt{1/4}$ mm
c_i	b_i mm
l	40 mm
l_b	30 mm
l_p	20 mm
v	25 mm/s [2, 16-17]
h	40 mm
p_i	0, 2, 4, 6, 7.95 Pa [11]
p_o	0 Pa
p_d	0, 1.0e^4, 2.0e^4, 3.0e^4, 3.5e^4 Pa
ρ_f	1030 kg/m^3 [18]
μ	1 cP [18-19]
ν	0.33
E	0.5 MPa [5]

3. Governing Equations and Boundary Conditions

The fluid flow problems introduced in this paper can be described through use of the conservation of mass and momentum equations. In two dimensions polar coordinates, the conservation of mass and the transient Navier-Stokes equations are arranged as

$$\frac{\partial u}{\partial r} + \frac{\partial w}{\partial z} = 0 \quad (1)$$

$$\rho \left(\frac{\partial u}{\partial t} \right) + \rho \left(u \frac{\partial u}{\partial r} + w \frac{\partial u}{\partial z} \right) = - \frac{\partial P}{\partial r} + \mu \left(\frac{\partial^2 u}{\partial r^2} + \frac{\partial^2 u}{\partial z^2} \right) \quad (2)$$

and

$$\rho \left(\frac{\partial w}{\partial t} \right) + \rho \left(u \frac{\partial w}{\partial r} + w \frac{\partial w}{\partial z} \right) = - \frac{\partial P}{\partial z} + \mu \left(\frac{\partial^2 w}{\partial r^2} + \frac{\partial^2 w}{\partial z^2} \right) \quad (3)$$

where \mathbf{u} and \mathbf{w} are the axial and radial velocities, respectively, noted in the coordinates \mathbf{z} and \mathbf{r} .

The variable \mathbf{p} is the force at the fluid-structure interface, acting along the stent and ureter walls, and throughout the fluid domain. The remaining variables density, ρ , and dynamic viscosity, μ , are properties of the fluid.

The fluid-structure boundary conditions are assumed as non-slip and can be defined radially as

$$\vec{u}(\mathbf{r}) = 0 \text{ when } \mathbf{r} = \{a_i, b_i, b_o, b_b\} \quad (4)$$

and axially, in the presence of a passage, as

$$\vec{u}(\mathbf{z}) = 0 \text{ when } \mathbf{z} = \left\{ \left(l_p - \frac{c_i}{2} \right), \left(l_p + \frac{c_i}{2} \right) \right\} \quad (5)$$

At the axis of symmetry the fluid velocity can be described by

$$\frac{du}{dr}(\mathbf{r}) = 0 \text{ for } \mathbf{r} = \{0\} \quad (6)$$

The open ends of the fluid domain are defined as inlet and outlet boundary conditions

$$p = f(z) \quad (7)$$

$$p(0) = p_i \text{ and } p(l) = p_o \quad (8)$$

At the fluid-structure interaction interface, the fluid exerts a total force on the boundary opposite that of the reaction force imposed on the fluid. This is noted as

$$\mathbf{f} = -\vec{n} \bullet (\rho \vec{I} + \mu(\nabla \vec{u} + (\nabla \vec{u})^T)) \quad (9)$$

This reaction force is in relation to the reference, undeformed mesh frame where the Navier-Stokes equations are defined in the spatial, deformed mesh. Because of this a transformation relationship is needed

$$\mathbf{F} = \mathbf{f} \bullet \frac{\partial v}{\partial V} \quad (10)$$

Where ∂v and dV are scale factors for the mesh elements in the spatial and reference frame, respectively. This relationship will determine how much force the fluid is exerting on the ureter wall, causing it to expand radially. The amount of deflection will be determined by this applied force and the defined properties of the ureter, such as the elastic modulus and Poisson's ratio, and is highly dependent on geometric shape and dimensions. Since the stent has been modeled as fixed and rigid, this boundary condition only exists for the interface between the fluid and ureter wall. The boundary condition for the outer radius of the ureter is a time dependent force profile that will deflect the ureter wall to act on the fluid in the local region of the maximum deflection, while allowing free deflection away from the deflection site. This equation is shown once more describing the outer ureter radius.

$$a_b(t) = p_d \bullet \exp(-(z - v^*t)^2 / (2^*(h/8)^2)) \quad (11)$$

The inner radius, a_i , is dependent on the outer radius and the wall thickness that results from strain developed in the region of deflection for every instance in time. The physical domain of the stent is allowed to deform freely with

boundary conditions at its ends limiting motion in the axial direction.

4. Numerical Simulation

The numerical simulations were completed using COMSOL 4.0 Multiphysics. The fluid and solid domains were coupled and modeled simultaneously. This allowed the use of the ureter walls as a motive force on the fluid while the fluid pressures generated could freely act to deflect its boundaries.

The combined domains for each model segment had approximately 9.2×10^4 elements. This number was approached on the conditions of geometry, element quality and solution accuracy. A mesh convergence study was conducted using progressively finer meshes to find the minimum number of elements required that, if doubled in density, yielded less than 1% difference in the solution of volumetric flow rates. For the geometry of the models presented, this value was found to be 6.4×10^4 . The solver used was a PARDISO, which is a parallel sparse direct linear solver that employed a backward differencing time stepping method for the transient flow simulations.

5.0 Results

5.1 Benchmark

In an effort to benchmark some fundamental steady state aspects of the model, results were compared with the work of Tong, Sparrow, and Abraham [11]. Geometric, material, and flow properties were matched for this exercise. The first flow scenario without a passage hole through the stent returned a solution of 19.0 ml/hr through the bore and 31.0 ml/hr through the annulus for a total of 50.0 ml/hr. Introducing a passage hole between the bore and annulus resulted in similar values of 19.3 ml/hr and 31.5 ml/hr in the bore and annulus respectively, both up and downstream of the passage, and totalled 50.8 ml/hr. These differences in flow rates matched those from the benchmark. When the blockage is introduced into the bore, the flow rates upstream of the passage hole are calculated to be 18.0 ml/hr and 29.5 ml/hr with downstream values of 14.0 ml/hr and 33.5 ml/hr in the bore and annulus respectively. This scenario revealed a reduction in total flow rate to 47.5 ml/hr.

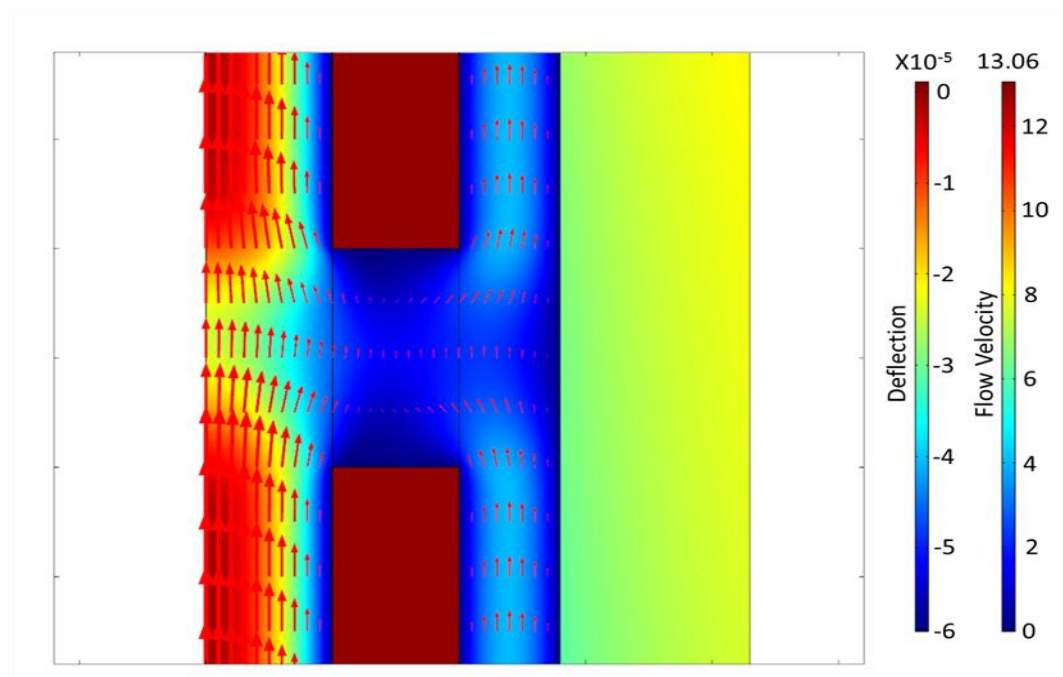


Figure 2: Flow velocities and directions through a stented ureter at passage without blockage.

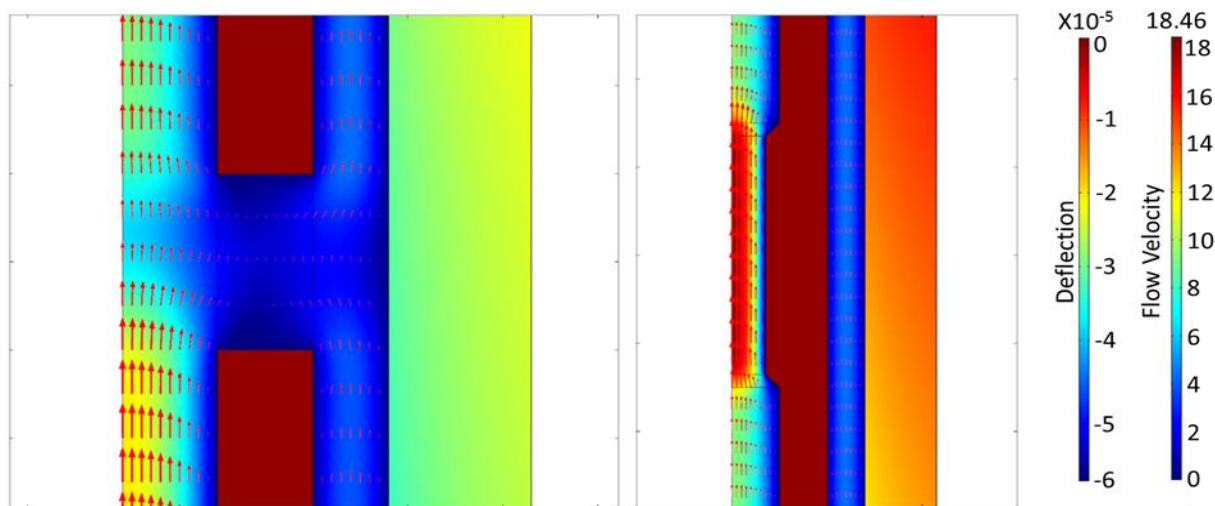


Figure 3: Flow velocities and directions through a stented ureter at passage (left) and with blockage (right).

Table 3: Matrix of Unobstructed Model Simulations

Increasing Pressure Difference Sweep →

		0 Pa	2 Pa	4 Pa	6 Pa	7.95 Pa
Increasing Wall Deflection Sweep ↓	0 %	0 Pa, 0 %	2 Pa, 0 %	4 Pa, 0 %	6 Pa, 0 %	7.95 Pa, 0 %
	22 %	0 Pa, 22 %	2 Pa, 22 %	4 Pa, 22 %	6 Pa, 22 %	7.95 Pa, 22 %
	44 %	0 Pa, 44 %	2 Pa, 44 %	4 Pa, 44 %	6 Pa, 44 %	7.95 Pa, 44 %
	65 %	0 Pa, 65 %	2 Pa, 65 %	4 Pa, 65 %	6 Pa, 65 %	7.95 Pa, 65 %
	75 %	0 Pa, 75 %	2 Pa, 75 %	4 Pa, 75 %	6 Pa, 75 %	7.95 Pa, 75 %

Figure 2 shows the magnitude and direction of the flow velocity near the passage hole using a colour scale, clearly demonstrating that no fluid passes between the bore and annulus in the absence of flow obstruction. When the blockage is implemented, a reduction in bore flow rate is apparent as evident in Figure 3, which shows the flow through the passage hole to the annulus. The blockage in the bore and the flow of fluid into the annulus creates increased pressure in both these regions upstream of the passage, restricting and reducing the flow as simulated.

5.2 Unobstructed Transient Flow

This section presents the results of peristaltic deflection on a stented ureter while varying the

degree of wall deflection and the pressure difference across the ureter segment without obstruction of the stent bore. Table 3 describes the simulations performed as a result of parallel parametric sweeps of the wall deflection and inlet pressure. From this point forward the properties of the fluid have been changed from those used in the benchmark to the values listed in Table 2, for urine at an average core body temperature of 37 °C.

Figure 4 shows the volumetric flow rates in the bore and annulus upstream and downstream of the passage hole, respectively, in reference to the position of the peristaltic deflection profile. These particular results are for a pressure difference of 7.95 Pa and a total radial wall deflection equal to

22 % of the total annulus thickness. The x-axis represents the position of the deflection profile, rather than time, to provide a clearer comparison to the accompanying geometric plots. Both figures show that, before the deflection profile enters the ureter segment, the flow rates are comparable to those at steady flow. However, they are not identical as expected with values of 18.0 and 28.5 ml/hr for the bore and annulus

respectively, totalling only 46.5 ml/hr. This difference is influenced entirely from the revision of fluid properties, from water to urine, and its reference temperature. This yielded a notable difference of 7%, considering the properties of urine are very close to that of water. It was thought that this high sensitivity in regards to fluid properties is related to the small scale of the system, nearing that of microfluidics.

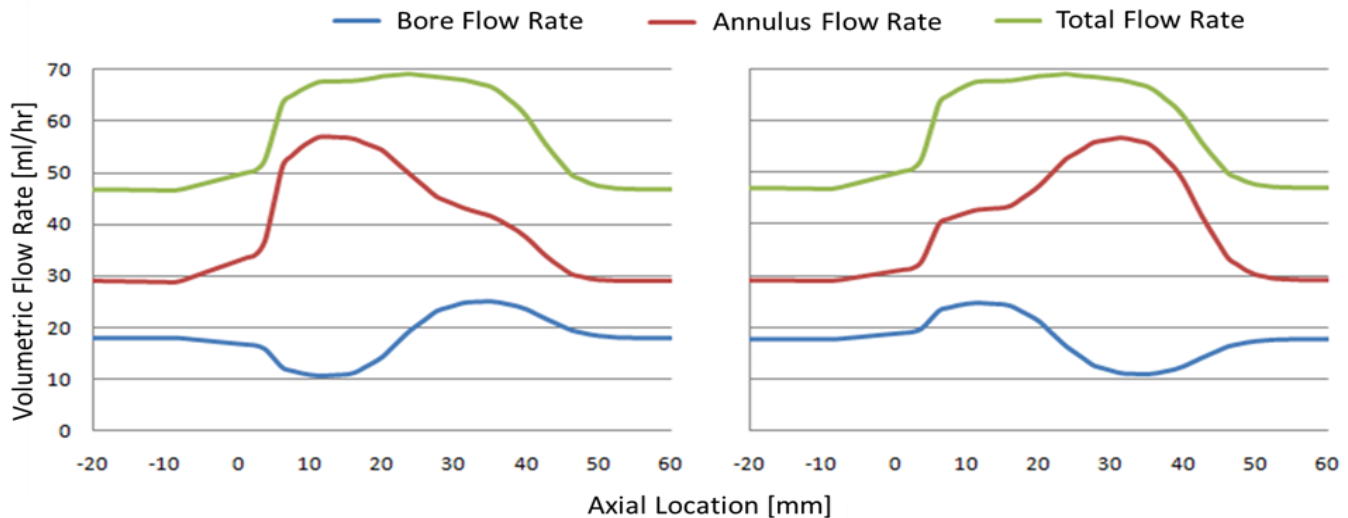


Figure 4: Upstream (left) and downstream (right) volumetric flow rates (Inlet pressure = 7.95 Pa, Deflection = 22 %).

Further analysis of the upstream flow rates in the figure above shows a rapid increase from steady state flow in the annulus as deflection is introduced to the model segment. As the profile transverse to the location of the passage hole, this flow rate reduces by the transfer of fluid into the bore until the wall deflection is downstream of the passage. At this point the flow rate gradually reduces to steady state value as the deflection profile leaves the ureter segment. The flow characteristics within the bore appear to be more symmetric not only about the passage, but also about its steady state flow rate. The increase and decrease of flow rate in the bore as peristalsis progresses along the ureter is opposite that of the annulus. The flow rate in the annulus always remains higher than the bore and their total approximates a symmetric curve against the position of the passage. Results for downstream flow rates mirror those of upstream about the passage hole location.

Figure 5 illustrates the velocity through the stented ureter while the wall deflection is upstream and downstream. This figure clearly indicates the change in flow rates as the deflection travels along the ureter. It is worthy of note that the direction of flow at any point shown in these images is always from the kidney to the bladder. Figure 6 may appear to contradict the prior statement where it is clear that fluid is travelling back upstream near the location of maximum deflection. This is a result of a high pressure region just ahead of the deflection and a low pressure region just behind the deflection, created as the profile pushes through the fluid. This is the essence of peristalsis; the high pressure region moves the fluid forward and the low pressure region pulls fluid in behind the travelling deflection. The fluid between these two regions will have a tendency to flow from regions of high pressure to low pressure, resulting in the localized backflow as shown.

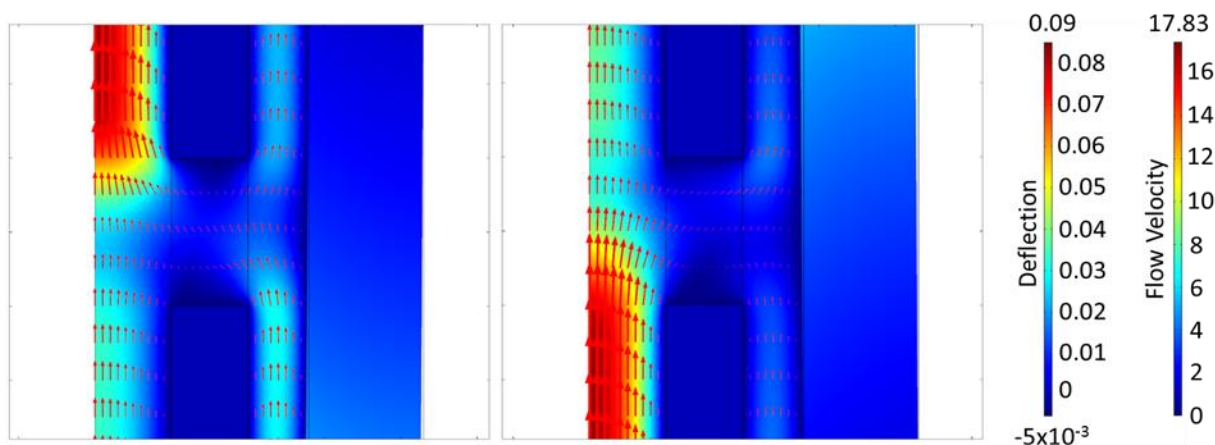


Figure 5: Flow at passage while peristalsis is upstream (left) and downstream (right). (Inlet pressure = 7.95 Pa, Deflection = 22 %).

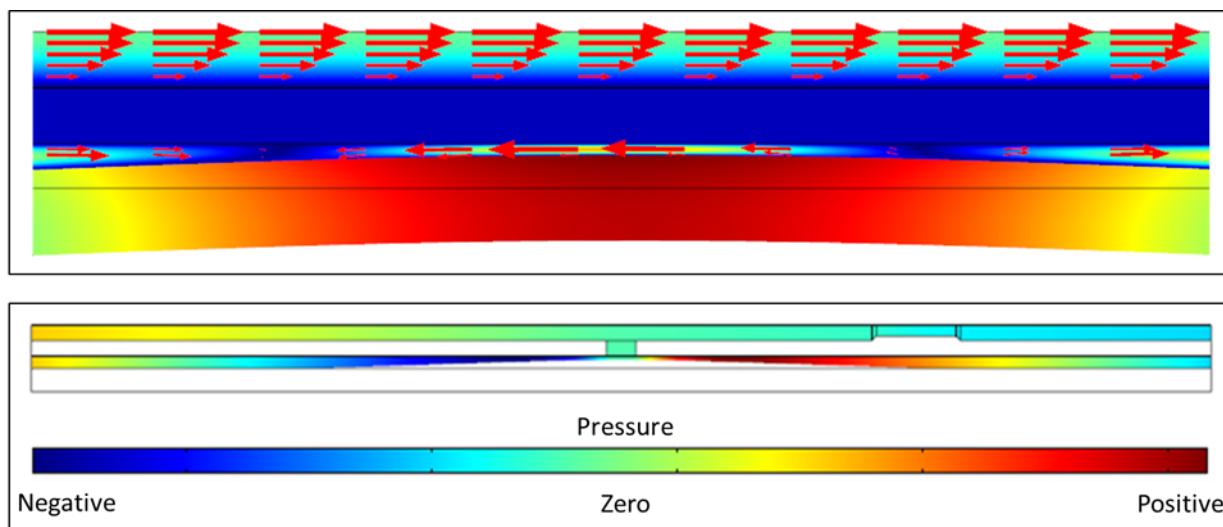


Figure 6: Local backflow near maximum wall deflection vs. pressure gradient.

As the pressure difference across the inlet and outlet of the ureter is reduced to zero, it is shown in Figure 7 that the flow rate in the bore has a negative magnitude for particular segments of the ureter where peristaltic deflection is present. Without a pressure difference between kidney and bladder, the high and low pressure regions created by peristalsis tend to push or pull fluid through the passage more readily.

If the pressure difference over the ureter segment was maintained at 7.95 Pa, and the maximum deflection increased to 75 % of the annulus thickness, the flow is described by Figure 8. These are the upstream and downstream portions of the model segment respectively. Initial

inspection reveals that the flow rate curves are not smooth as those in Figures 4 and 7. This may be attributed to the integration that is performed on the highly deformed fluid domain mesh while the deflection profile is active. An interesting event occurs as the wall deflection moves over the stent passage hole. As the local high pressure region created by the deflection moves beyond the passage, the fluid being displaced from this region moves principally in the path of least resistance; toward the ureter terminus at the bladder. This will result in higher downstream annular flow rates and will reduce the opposition to inlet pressure at the kidney allowing for higher upstream bore flow rates. As the local low

pressure region moves towards the passage hole, fluid is drawn through the annulus and bore more readily towards this position. Between these two locations of peristalsis is where the spike in total flow rate occurs on the plots. While the deflection profile moves further downstream, the annulus pressure near the passage begins to increase once again to oppose the flow through the bore and reduce the overall flow rate. Another characteristic visible in the total flow curve are the values on either side of the spike. The total flow while the deflection is downstream of the passage is clearly larger than that while it is upstream.

This is owing to the opposition to the inlet pressure while the high pressure region is upstream of the passage hole, thus reducing total flow. Once the low pressure region moves downstream a pressure gradient over the passage hole is generated in favour of the inlet pressure resulting in higher total flow. One final comment for this figure is that there are negative flow rates for the bore, suggesting reflux is occurring even at an inlet pressure of 7.95 Pa and will grow severely as this pressure is reduced. Figure 9 quantifies the flow of fluid through the stented ureter while the deflection moves past the passage.

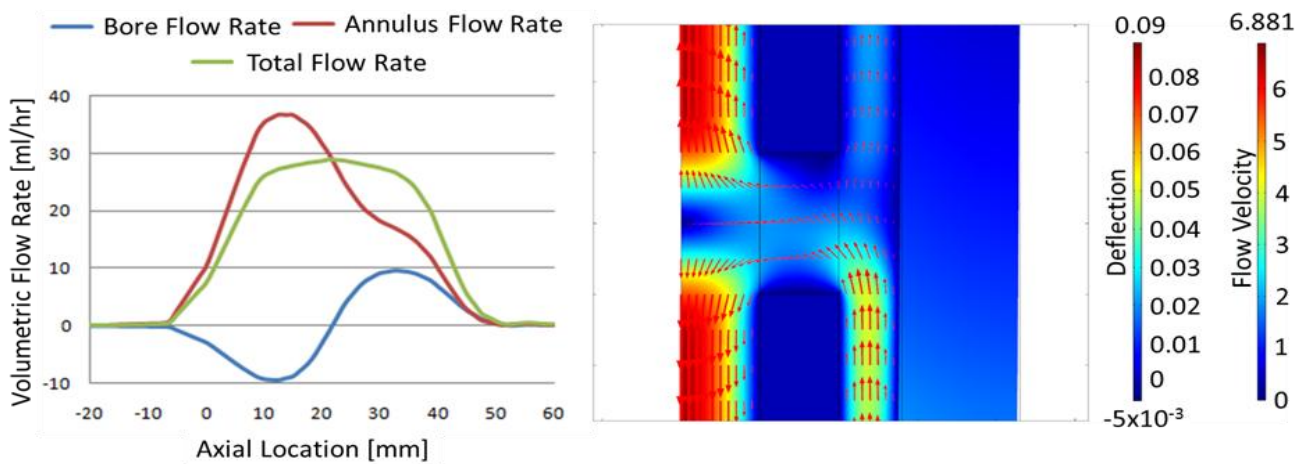


Figure 7: Upstream volumetric flow rate and direction (Inlet pressure = 0 Pa, Deflection = 22 %).

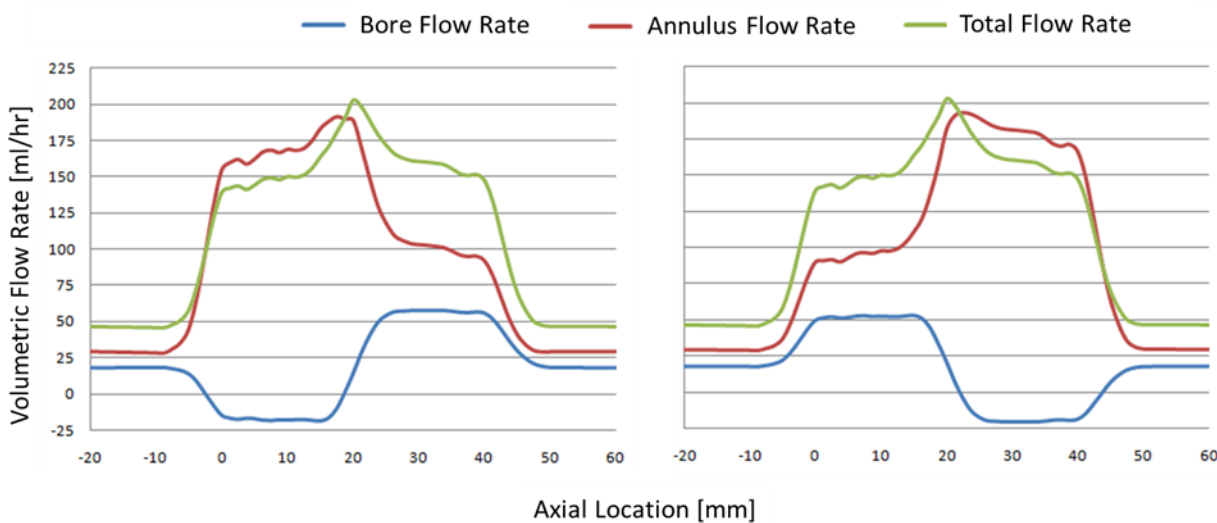


Figure 8: Upstream (left) and Downstream (right) volumetric flow rate (Inlet pressure = 7.95 Pa, Deflection = 75 %).

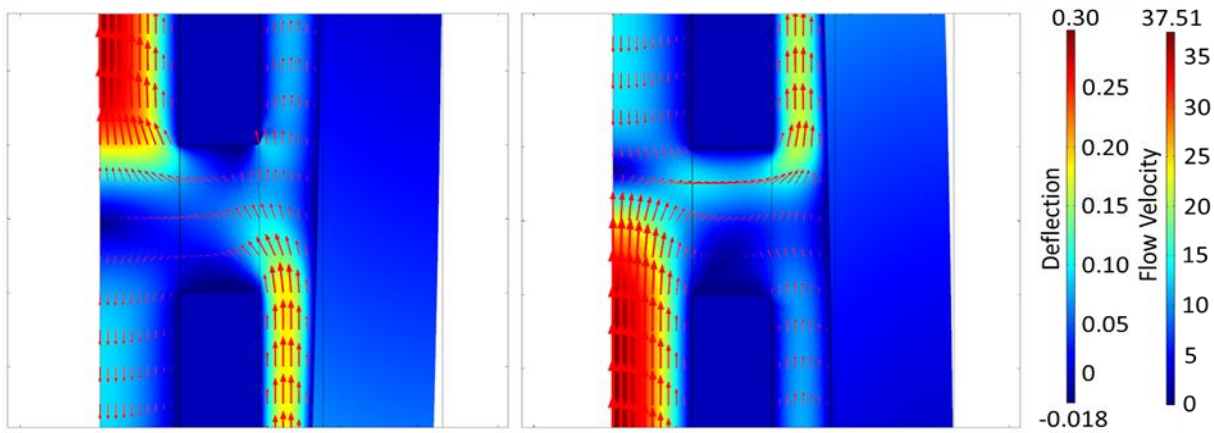


Figure 9: Flow at passage while peristalsis is upstream (left) and downstream (right) (Inlet pressure = 7.95 Pa, Deflection = 75 %).

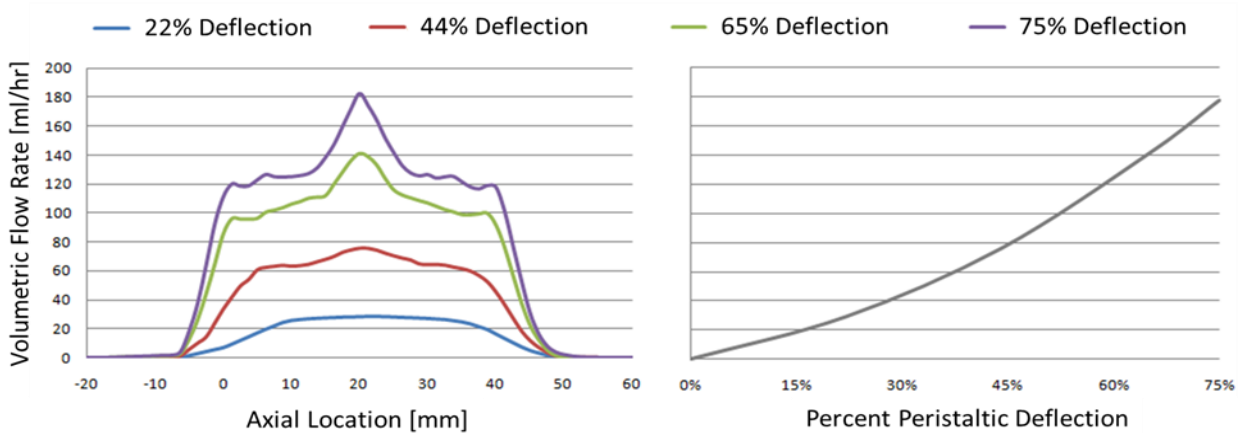


Figure 10: Total flow rate influenced by peristaltic deflection (Inlet pressure = 0 Pa)

It has been shown that increases in total flow rate through the stented ureter with passage holes are directly related to increases in the depth of peristaltic deflection. Changing this input value by sweeping its parametric value during simulation yields results shown in Figure 10 while inlet pressure remains constant. Not only does the total flow rate increase with larger peristaltic deflection but so does the magnitude of the spike in total flow as the deflection moves past the stent passage hole. There is a nonlinear relationship between the depth of deflection and the value for peak total flow rate that results.

Figure 11 illustrates that as the inlet pressure increases the peak and total flow rates follow in a linear fashion. To compare the results of varying inlet pressure to that of peristaltic depth, Figure 12 shows a linear curve that represents a threshold to the onset of reflux. Any point under the curve represents combinations for pressure difference and peristaltic depth for this particular geometric scenario that will produce downstream flow from the kidney to the bladder over the entire transient simulation.

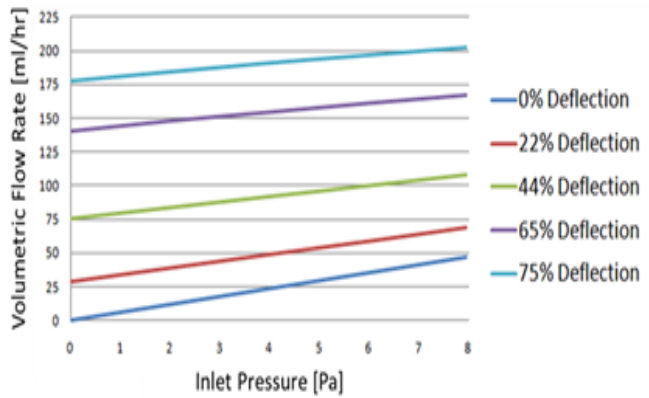


Figure 2: Change in flow rate vs. pressure difference as deflection is increased.

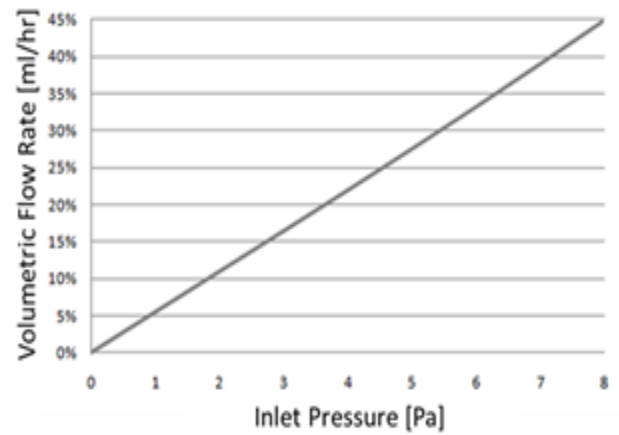


Figure 3: Parameter value limits in avoiding fluid reflux.

Table 4: Matrix of Obstructed Model Simulations

Increasing Bore Blockage Sweep →

		0 %	25 %	50 %	75 %
Increasing Wall Deflection Sweep	0 %	0 %, 0 %	25 %, 0 %	50 %, 0 %	75 %, 0 %
	22 %	0 %, 22 %	25 %, 22 %	50 %, 22 %	75 %, 22 %
	44 %	0 %, 44 %	25 %, 44 %	50 %, 44 %	75 %, 44 %
	65 %	0 %, 65 %	25 %, 65 %	50 %, 65 %	75 %, 65 %

5.3 Obstructed Transient Flow

This section discusses the results of peristaltic deflection of a stented ureter while varying the degree of wall deflection and the blockage of the bore downstream of the stent passage hole for a pressure difference across the ureter segment of 7.95 Pa. Table 4 describes the simulations performed as a result of parallel parametric sweeps of the wall deflection and bore blockage.

Before the effects of obstructing the bore on transient flow are introduced, a discussion of these blockages in steady flow is made. An examination of no blockage in the segment reveals a linear relationship between the flow rates and

pressure differential for all axial locations. In terms of percentages, the bore delivers 38% of the flow rate while the annulus supplies the remainder. As blockage is introduced, the proportions of flow rate throughout the model differ upstream and downstream as supported by Figure 13. The percentage flow rate distribution is constant upstream of the passage hole for any size blockage and reduce proportionally as flow restriction increases such as in Figure 14. Proportions will increase in favour of the annulus as a downstream blockage in the bore is increased.

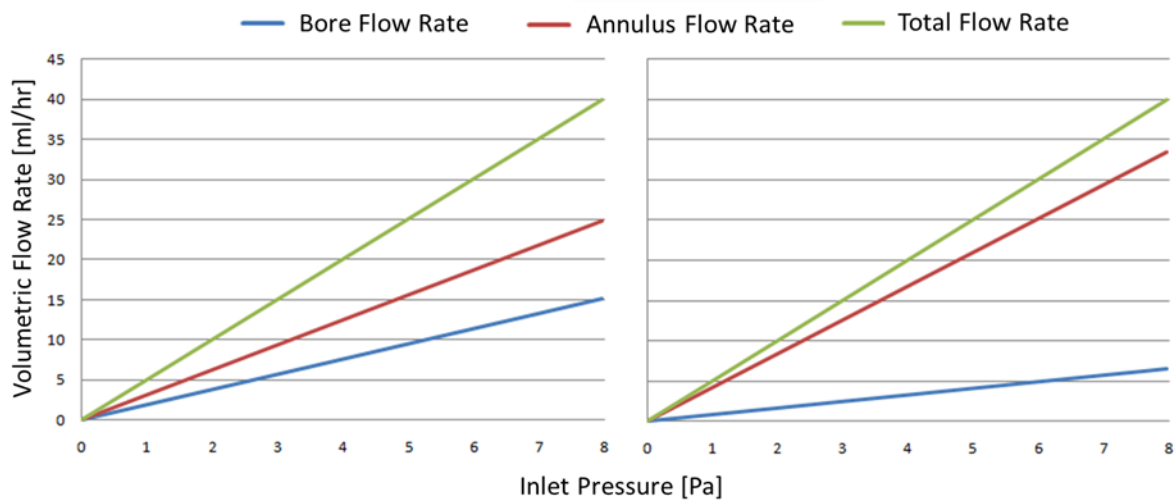


Figure 4: Change in steady state flow rate vs. pressure upstream (left) and downstream (right) of passage (Blockage = 75%).

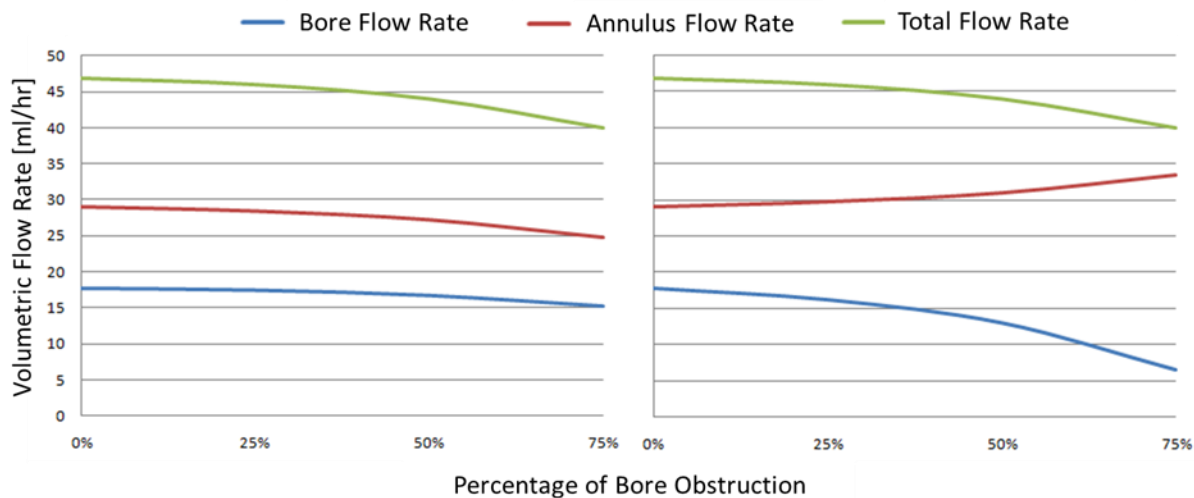


Figure 5: Change in steady state flow rate vs. blockage upstream (left) and downstream (right) of passage (Inlet Pressure = 7.95 Pa).

The transient effects of peristaltic deflection are now analyzed. The results from varying the percentage of bore obstruction while using a ureteral deflection of 65% reflect those discussed in the unobstructed transient flow. The effects of increasing the blockage to 75% of the bore have very similar flow rate characteristics as unobstructed flow depicted previously in Figure 8. It appears that the flow rate upstream of the passage hole does not maintain the constant annulus/bore ratios determined in the steady state analysis. However, if the mean flow value of each fluid domain is evaluated while peristaltic

deflection is downstream of the passage hole, the results reflect those of steady state. The constant upstream ratios are near those of steady state but with slightly more weight in the annulus flow. This is expected as the local high pressure region positioned downstream of the passage would act against the pressure force in the bore.

The ratios of flow downstream of the passage while the deflection is in this region become heavily weighted through the annulus as bore obstruction is increased. The nonlinear relationship of the annulus flow rate moves from an upward trend seen in Figure 14 to a downward

trend as the peristaltic deflection is increased. Because of this the deflection of the ureter wall itself can be viewed as an obstruction within the annulus, under the conditions that the pressure gradient behind the deflection is large enough to generate an annulus flow rate greater than that of peristalsis on its own. It is perceived that the effectiveness of the stent is reduced in the presence of peristalses for a sufficient combination of blockage and pressure difference. Going back to Figure 10 and 11 shows that strong deflection in unison with a pressure gradient creates far higher total flow rates than pressure on its own. Introducing blockage to this relationship would likely bring these curves to a more linear relationship or possibly a negative concavity resulting in a reduced, yet still significant, increase in combined flow rate.

Analyzing the upstream and downstream flow trends while peristalsis is upstream is performed in the same fashion as when it was evaluated downstream. For the upstream flow relationships, the bore will tend to experience reflux as peristaltic deflection increases and is further encouraged with the addition of downstream bore obstruction. This is the result of higher flow restrictions generated by the blockage creating higher pressures at the passage therefore impeding the flow in this domain. The lower flow through

the passage from the bore allows for a larger flow rate of fluid through the annulus across the passage. The downstream flow percentages are very similar to those of the steady state analysis with the slight positive offset in annulus flow rate owing to the higher back pressures at the blockage.

Figure 15 compares the total flow rate curves resulting from bore obstruction while inlet pressure is 7.95 Pa and deflection is 65 % of annulus thickness. The presence of a blockage increases the effect that peristalsis has on the total flow rate where the value is higher when the deflection is downstream of the stent passage than when it is upstream. The blockage results in a reduction for all instances of peristalsis where deflection is low. However, Figure 15 shows a slight increase downstream when deflection is high. Once again a threshold is determined to estimate the combination of percent obstruction and percent deflection that would result in reflux and is provided in Figure 16. The relationship is a nonlinear one where the required percentage of wall deflection resulting reflux reduces as the percentage of bore blockage is increased. This figure also includes several curves for lower pressure gradients illustrating that, as the pressure differences reduce, a lesser deflection is needed to generate reflux within this model.

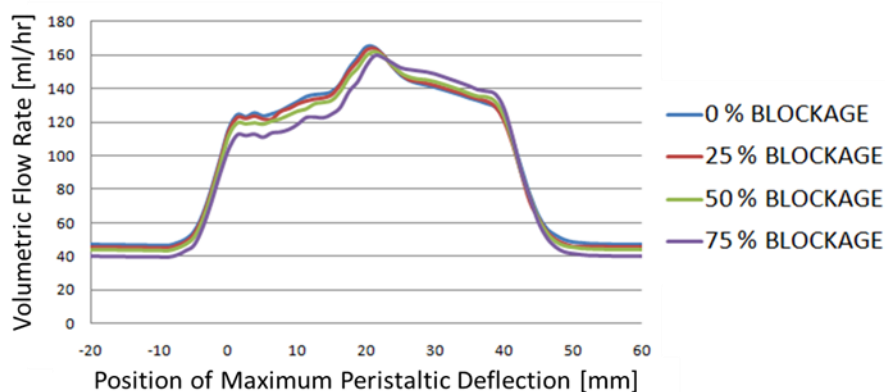


Figure 6: Total flow rate influenced by bore obstruction (Deflection = 65 %).

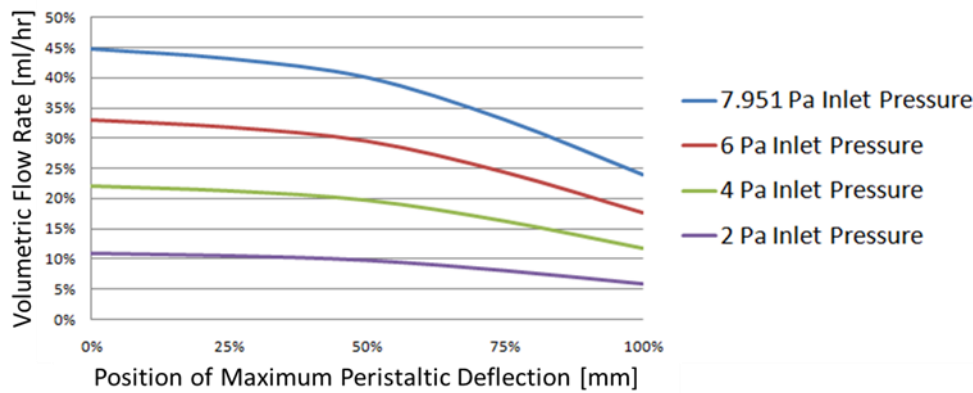


Figure 7: Parameter value limits in avoiding fluid reflux.

6. Conclusions and Recommendations

◆ The results of this study have revealed a distinct risk of reflux while peristalsis is present within a stented ureter. It was found that an increase in bore (lumen) obstruction within the stent or the amplitude of peristaltic wave in the ureter can generate reflux through the bore. The risk is highest at initial passages near the kidney such that the reflux upstream of the deflection profile is reduced at every passage between its position and the proximal end of the ureter. There is possibility of reflux under weak peristalsis if the pressure gradient along the ureter diminishes; this possibility is enhanced in the presence of obstruction due to encrustation or biofouling.

◆ The analysis of the simulations illustrated relationships between key variables for generic dimensions of a typical stent construction. The methods employed in determining these relationships can be applied to many stent geometries and could serve as a valuable tool for stent design.

◆ Future research is recommended in the context of stent geometry and blockages, as well as blockage locations throughout the annulus and bore of a stented ureter. Additional studies of the effects of peristalsis could be conducted by varying the velocity or profile of the deflection. A three-dimensional study of the entire stented ureter length could provide a more realistic illustration of the fluid behaviour as it traverses the ureter length. The material and model used for the ureter wall

could be selected to better represent the non-linear, viscoelastic properties of the tissue.

Acknowledgments

This research was supported through NSERC Discovery funding.

References

- [1] Lam, J.; Gupta, M., Update on Ureteral Stents, *Urology*, 2004, 64, 9-15. DOI: [10.1177/1756287210370699](https://doi.org/10.1177/1756287210370699)
- [2] Kinn, A.; Lykkeskov-Andersen, H., Impact on Ureteral Peristalsis in a Stented Ureter An Experimental Study in the Pig, *Urological Research*, 2002, 30, 213-218.
- [3] Denstedt, J.; Reid, G.; Sofer, M., Advances in Ureteral Stent Technology, *World J Urol*, 2000, 18(4), 237-242. DOI: [10.1007/PL00007074](https://doi.org/10.1007/PL00007074)
- [4] Waters, S.; Heaton, K.; Siggers, J.; Bayston, R.; Bishop, M.; Cummings, L; Grant, D; Oliver, J.; Wattis, J., Ureteric Stents: Investigating Flow and Encrustation, *Journal of Engineering in Medicine*, 2008, 222(4), 551-561. DOI: [10.1243/09544119JEIM317](https://doi.org/10.1243/09544119JEIM317)
- [5] Vahidi, B.; Fatourae, N., A Numerical Simulation of Peristaltic motion in the Ureter Using Fluid Structure Interactions, *Conference of the IEEE EMBS*, 2007, 29, 1168-1171.

- [6] Saltzman, B., Ureteral Stents, Indications, Variations and Complications, *Urologic Clinics of North America*, 15(3), 1988, 481-491.
- [7] Ezz-El-Deen, M.; Khalaf, I.; Abdel Rahim, F., Effect of Internal Ureteral Stenting of Normal Ureter on the Upper Urinary Tract: An Experimental Study, *Journal of Endourology*, 7(5), 1993, 399-405.
- [8] Franco, G.; De Dominicis, C.; Dal Forno, S.; Iori, F.; Laurenti, C., The Incidence of Post-operative Urinary Tract Infection in Patients with Ureteric Stents, *British Journal of Urology*, 65(1), 1990, 10-12. DOI: [10.1111/j.1464-410X](https://doi.org/10.1111/j.1464-410X)
- [9] Hübner, W.; Plas, E.; Trigo-Rocha, F.; Tanagho, E., Drainage and Reflux Characteristics of Antireflux Ureteral Double-J Stents, *Journal of Endourology*, 7(6), 1993, 497-499. DOI: [10.1089/end.1993.7.497](https://doi.org/10.1089/end.1993.7.497).
- [10] Payne, S.; Ramsay J, The Effects of Double J Stents on Renal Pelvic Dynamics in the Pig, *Journal of Urology*, 140(3), 1988, 637-641.
- [11] Tong J.; Sparrow, E.; Abraham, J., Numerical Simulation of the Urine Flow in a Stented Ureter, *Journal of Biomechanical Engineering*, 129(2), 2007, 187-192.
- [12] Siggers, J.; Watters, S.; Wattis, J.; Cummings, L., Flow Dynamics in a Stented Ureter, *Mathematical Medicine and Biology*, 2008, 1-24. DOI: [10.1093/imammb/dqn020](https://doi.org/10.1093/imammb/dqn020)
- [13] Ramsay, J.; Payne, S.; Gosling, P.; Whitfield, H.; Wickham, J.; Levison, D., The Effects of Double-J Stenting on Unobstructed Ureters. An Experimental and Clinical Study, *British Journal of Urology*, 57(6), 1985, 630-634. DOI: [10.1111/j.1464-410X.1985.tb07021.x](https://doi.org/10.1111/j.1464-410X.1985.tb07021.x)
- [14] Tsuchaiya, T.; Takei, N, Pressure Responses and Conduction of Peristaltic Wave in Guinea-Pig Ureter, *Japanese Journal of Physiology*, 40(1), 1990, 139-149.
- [15] Rose, J.; Gillenwater, J., Pathophysiology of ureteral obstruction, *American Journal of Physiology*, 225(4), 1973, 830-837.
- [16] Griffiths, D.; Constantinou, C.; Mortensen, J.; Djurhuus, J., Dynamics of the Upper Urinary Tract: II. The Effect of Variations of Peristaltic Frequency and Bladder Pressure on Pyeloureteral Pressure/flow Relations, *Physics in Medicine and Biology*, 32(7), 1987, 823-833. DOI: [10.1088/0031-9155/32/7/003](https://doi.org/10.1088/0031-9155/32/7/003)
- [17] Venkatesh, R.; Landman, J.; Minor, S.; Lee, D.; Rehman, J.; Vanlangendonck, R.; Ragab, M.; Morrissey, C.; Clayman, R., Impact of a Double-Pigtail Stent on Ureteral Peristalsis in the Porcine Model: Initial Studies Using a Novel Implantable Magnetic Sensor," *Journal of Endourology*, 19(2), 2005, 170-176. DOI: [10.1089/end.2005.19.170](https://doi.org/10.1089/end.2005.19.170).
- [18] Adler, R.; Rubin, J.; Price, C., Interpretation of Submerged Laminar Jets: Ureteric Jet Phenomenon, *Radiology*, 178(3), 1991, 888-889.
- [19] Burton-Opitz, R.; Dinegar, R., The Viscosity of Urine, *American Journal of Physiology*, 47(2), 1918, 220-230.